Discrete & Computational Geometry
https://doi.org/10.1007/s00454-023-00525-w

Uniformly Acute Triangulations of Polygons

Christopher J. Bishop[1]

Received: 18 August 2021 / Revised: 6 July 2022 / Accepted: 8 August 2022

Abstract
We show that any polygon Γ has an acute triangulation $\mathcal{T}$ where every angle lies in the interval $[30°, 75°]$, except for triangles that contain a vertex v of Γ where Γ has an interior angle $\theta_v < 30°$; such triangles are isosceles with angles θ_v, and $90° - \theta_v/2$.

Keywords Acute triangulation · Optimal meshing · Steiner points · Conformal maps · Schwarz–Christoffel formula

Mathematics Subject Classification 68U05 · 52B55 · 68Q25

1 Introduction

A polygon is a Jordan curve P in the plane consisting of a finite number of distinct vertices $V = \{z_1, \ldots, z_n\}$ and open segments $\{(z_1, z_2), \ldots, (z_{n-1}, z_n), (z_n, z_1)\}$ that are pairwise disjoint. The bounded connected component of $\mathbb{R}^2 \setminus P$ is called the interior of P and is denoted $\text{Int}(P)$; for brevity we will often call this open domain Ω. The domain's closure is $\overline{\text{Int}(P)} = \text{Int}(P) \cup P$; this will be called the polygonal region associated to P. A polygon with three vertices is a triangle, and when the meaning is clear from context, we will abuse notation and refer to both the curve and the closed triangular region it bounds as "triangles".

A triangulation of a polygon P is a finite collection $\{T_k\}$ of triangular regions contained in $\overline{\text{Int}(P)}$ such that: (1) the union covers $\overline{\text{Int}(P)}$, (2) the triangles have disjoint interiors, and (3) the triangles have the simplex property: any two triangles are

Editor in Charge: János Pach

Data sharing not applicable to this article as no datasets were generated or analyzed during the current study. The author is partially supported by NSF Grant DMS 1906259.

Christopher J. Bishop
bishop@math.stonybrook.edu

[1] Mathematics Department, Stony Brook University, Stony Brook, NY 11794-3651, USA

Published online: 21 July 2023

either disjoint, intersect in a single point which is a vertex of each triangle, or intersect in a segment that is an edge of each triangle. The triangles may have vertices other than those of P, and these "extra" vertices are called the Steiner points of the triangulation. Given a polygon P, finding triangulations (with or without Steiner points) with few elements and/or nice geometric properties is a fundamental problem of computation geometry. In this paper, we are concerned with the geometric question: if we allow any number of elements, what is the smallest angle θ such that every polygon P has a triangulation with almost every angle $\leq \theta$? (The meaning of "almost" will be explained below.) If we insist on bounding every angle of the triangulation, then $\theta = 90^\circ$ is the best we can hope for. It is known that every polygon has an acute triangulation (all angles $< 90^\circ$) e.g., see [1, 11, 30, 35]. If P has a vertex v with small interior angle θ_v, then any triangulation of P has a triangle T containing v and this triangle must have an angle $\leq \theta_v$, and hence another angle $\geq 90^\circ - \theta_v/2$. Thus no uniform angle bound strictly less than 90° can hold. However, such a bound holds if we simply ignore one triangle for each "small" vertex, i.e., $\theta_v < 30^\circ$.

Theorem 1.1 *Every polygon P has a triangulation $\mathcal{T}$ such that every triangle T in $\mathcal{T}$ has its angles in the interval* $[30^\circ, 75^\circ]$*, unless T contains a vertex v of P with interior angle $\theta_v < 30^\circ$; then T is isosceles with angles θ_v and $90^\circ - \theta_v/2$.*

A triangulation using only angles $\leq \phi$ is called a ϕ-triangulation. A ϕ-triangulation is called non-obtuse if $\phi = 90^\circ$ and is called acute if $\phi < 90^\circ$. Theorem 1.1 implies every polygon has a ϕ-triangulation with $\phi = 90^\circ - \min(30^\circ, \theta_{\min})/2$, where $\theta_{\min}$ is the minimum interior angle of P. A stronger bound is possible: [8] proves that every polygon has a ϕ-triangulation with $\phi = 90^\circ - \min(36^\circ, \theta_{\min})/2$, and that this bound is sharp. The bound is a consequence of a more general result in [8] that computes $\Phi(P) = \inf\{\phi : P \text{ has a } \phi\text{-triangulation}\}$ for any given polygon. However, Theorem 1.1 is not a corollary of this result because the construction given in [8] can create multiple triangles with angles outside $[36^\circ, 72^\circ]$ for each angle of P that is less than 36°, whereas Theorem 1.1 creates just one triangle with angles outside $[30^\circ, 75^\circ]$ for each vertex with angle $< 30^\circ$.

To explain the distinction more carefully, I will (very) briefly review the construction in [8]. It divides the interior of P into a finite number of pieces, and on each piece the triangulation is defined as the image of a nearly equilateral triangulation of a corresponding "model region" under a conformal map. Each vertex $v \in P$ is associated to a piece that is a small truncated sector with vertex v and angle θ_v, the interior angle of P at v. The corresponding model region is another sector whose angle ψ_v is an appropriate integer multiple of 60°, and such a sector has a natural triangulation by equilateral triangles. The conformal map between the sectors is a power map $z \mapsto a + bz^\alpha$ with $\alpha = \theta_v/\psi_v$. Angles of triangles touching v are distorted by a factor of α, but the distortion diminishes as the distance to v increases; see Corollary 3.3. Far enough from v the image triangles are nearly nearly equilateral, and can easily be merged with the triangulation of an adjacent piece of the polygon. Thus several angles $> 72^\circ$ may occur near v; numerical experiments indicate six exceptional triangles can occur as $\theta_v \searrow 0$. Theorem 1.1 reduces this to just one exceptional triangle per small vertex by increasing the angle bound from 72° to 75°.

Remark 1 Theorem 1.1 is the triangular analog of a result for quadrilateral meshes in [6]: every polygon P has a quadrilateral mesh with all angles in $[60°, 120°]$, except for quadrilaterals that contain a vertex v of P where the interior angle is $\theta_v \leq 60°$. The exceptional quadrilaterals are kites with opposite angles θ_v and $120°$, and the remaining pair of opposite angles are both equal to $120° - \theta_v/2$.

Remark 2 Theorem 1.1 is also the polygonal version of a result for planar straight line graphs (PSLGs) given in [9]. That paper proves that there is a $\theta_0 > 0$ such that every PSLG Γ has a conforming triangulation with all angles in $[\theta_0, 90° - \theta_0/2]$, except for triangles containing a vertex v of Γ with interior angle smaller than θ_0. Such triangles are isosceles with angles in $[\theta_v, 90° - \theta_v]$ where θ_v is the minimum interior angle of Γ at v (a PSLG may have more than one angle at a vertex). In particular, a PSLG with minimum angle $\theta_{\min}$ has a conforming triangulation with all angles $\leq 90° - \min(\theta_0, \theta_{\min})/2$. The argument for PSLGs in [9] is significantly more involved than the proof for polygons given here. It depends on compactness, so it does not give an explicit value for θ_0 (the optimal value remains unknown). One purpose of this paper is to show that the argument simplifies in the special case of polygons, and that we can obtain the explicit value $\theta_0 = 30°$.

Remark 3 Finding acute triangulations of polygons and PSLGs has a long history and many applications, e.g., see [7] or [41] for lists of algorithms that work better with acute or non-obtuse triangulations. Very briefly, in 1960 Burago and Zalgaller [11] showed that any polyhedral surface has an acute triangulation. See also [12]. In 1984 Gerver [19] used the Riemann mapping theorem to show that if a polygon's angles all exceed 36°, then there exists a dissection of it into triangles with maximum angle 72° (a dissection satisfies conditions (1) and (2) of a triangulation, as defined earlier, but not (3)). He conjectured an optimal angle bound for dissections of arbitrary polygons, and this was later proven in [8]. In 1988 Baker et al. [1] rediscovered (a weaker form of) the Burago–Zalgaller theorem, by proving that any polygon has a nonobtuse triangulation, and their construction also gave a lower angle bound in some cases. In 2002 Maehara [30] showed that any nonobtuse triangulation with N triangles can be refined to an acute triangulation with $O(N)$ elements. Thus finding an acute triangulation (angles $< 90°$) reduces to finding a nonobtuse one (angles $\leq 90°$). A different proof of this was given by Yuan in [37], and also by Saraf [35]. Besides the papers cited earlier, a few other highlights and surveys of the theory include [2–5, 7, 16, 18, 20, 27, 32, 34]. The problem of acutely triangulating particular polygons has arisen in recreational mathematics, e.g., finding the smallest acute triangulation of a square (it uses eight triangles) is considered by Lindgren [28] and Cassidy and Lord [13]. Eppstein [17] discusses optimal angle bounds for triangulating a square, a question of John Tromp from a 1996 `sci.math` post. Eppstein mentions that Gerver proved 72° is optimal for dissections, but Gerver also proved it is optimal for triangulations (see [19, Fig. 4]). (Surprisingly, the optimal bounds for dissections and triangulations are the same for any polygon; see [8, Cor. 1.3].) Acute triangulations of other shapes and surfaces are considered in [21–24, 29, 31, 38–40]. Higher dimensional analogs are extremely interesting but much more difficult, e.g., the best known acute triangulation of the 3-cube has thousands of tetrahedron. See [10, 25, 26].

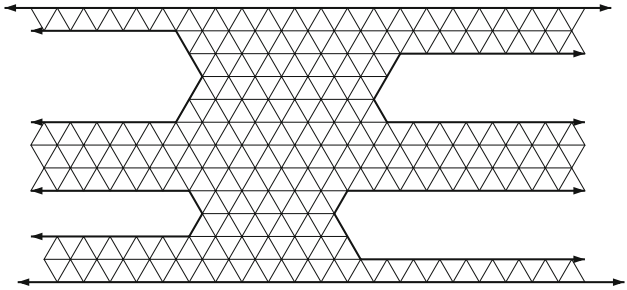

Fig. 1 A model domain is a subset of an infinite strip that has several closed regions removed. Each closed region is bounded by an unbounded Jordan curve consisting of two horizontal infinite rays and two finite segments and has three angles of 120°. In this figure, the model domain has an equilateral triangulation, although most model domains only have nearly equilateral triangulations (see Lemma 2.1). In this picture there are six infinite ends: three go left, three go right, and there are two ends each of thicknesses 1, 2, and 3

I thank the two anonymous referees for their detailed and thoughtful reports, which provided numerous concrete suggestions for improving the exposition of the paper.

2 Model Domains

As noted in the introduction, the general idea used in this paper is the same as in [8]: given a polygon P we construct another polygon P' and a conformal map between their interiors. The model polygon P' is chosen so that its interior has an nearly equilateral triangulation (defined below). Away from the vertices of P, the conformal map between P' and P nearly preserves the shape of these triangles, and this gives a nearly equilateral triangulation of P away from its vertices; a separate construction is needed in a neighborhood of each vertex.

Unlike the construction in [8], where P' is chosen to be a finite polygon, the P' we use in this paper is unbounded, and thus not a polygon at all, in the sense of the first paragraph of this paper. The interior of P' is of the form

$$\Omega' = \mathrm{Int}(P') = (\mathbb{R} \times [0, 1]) \setminus \bigcup_{k=1}^{n} U_k,$$

where the $\{U_k\}$ are pairwise disjoint, closed, unbounded subsets of $S = \mathbb{R} \times [0, 1]$. Each U_k is bounded by an unbounded Jordan arc (a homeomorphic, proper image of $\mathbb{R} \to \mathbb{R}^2$) containing two infinite horizontal rays, whose finite endpoints are joined by a polygonal arc consisting of two finite line segments, so that all three interior angles of U_k are 120°. See Fig. 1.

Given a polygon P with n vertices, the model P' will be chosen to have n infinite ends and so that there is a conformal map f sending each infinite end of P' to a vertex of P: more precisely, this means that as $z \to \infty$ through one of the ends of Ω', $f(z)$ tends to a vertex of P. This condition imposes restrictions on how P' can be chosen, since a conformal map between general simply connected domains only allows three boundary points to have specified images; requiring n boundary points match up

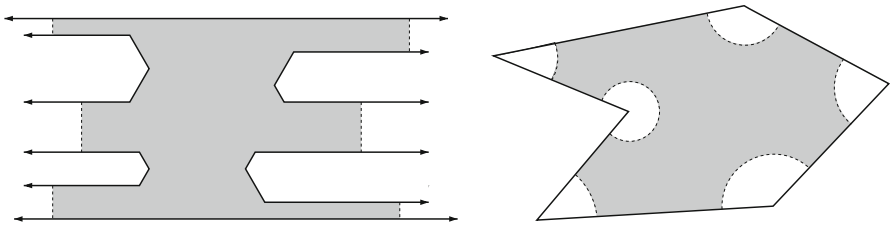

Fig. 2 We use the conformal map to transfer a nearly equilateral triangulation from a compact region of the model domain (shaded) to the interior of P minus neighborhoods of each vertex. We then have to triangulate the neighborhoods and make the meshes match up

requires a very special choice of P'. Fortunately, such a P' can be constructed using the Schwarz–Christoffel formula, as discussed in Sect. 3.

The model domain in Fig. 1 is shown with an equilateral triangulation. In general, not every model domain has an equilateral triangulation; it is easy to see that only countably many model domains can have one. However, every model domain has a nearly equilateral triangulation. This means that for any $\epsilon > 0$ we can choose a triangulation with all angles in $[60^\circ - \epsilon, 60^\circ + \epsilon]$, and so that only finitely many triangles are not equilateral (so for our model domains, the triangulation becomes equilateral far enough down each infinite end). The following simple fact is left to the reader (a very similar result is proven in [8, Sect. 5]).

Lemma 2.1 *Every model domain has nearly equilateral triangulations.*

Given a nearly equilateral triangulation of a model domain, the "thickness" of an infinite end is the number of triangles needed to connect the top and bottom sides of the end, i.e., the number of horizontal rows of triangles in the end. By sub-diving triangles, we can clearly make these thicknesses as large as we wish. For our construction, we need to specify the thickness of each end independently of the other ends, and in Sect. 4 we will see how to do this.

When we conformally map the model P' to the given domain P, the images of the nearly equilateral triangulation will give a triangulation of P, except near the vertices of P. Since the triangulation of P' has an infinite number of triangles in each infinite end, we will only transfer the part of the triangulation inside a bounded subset of the model defined by cutting each end with a vertical line segment S far enough out the end that the triangulation near S is equilateral. The cut-off half-strip maps to a sector at the corresponding vertex of P. See Fig. 2. The vertical segment at the end of the half-strip is not covered by edges of the triangulation, so we will have to "fill in" a triangulation between the equilateral triangulation the end and the vertical segment. This is also explained in Sect. 4. After that, we give an explicit construction that extends the image triangulation into these sectors at each each vertex v, being careful that no angles $> 75^\circ$ are used, except for one triangle that touches v (and only then if the angle at v is $< 30^\circ$). This construction depends heavily on numerical computations of angles for explicit families of triangulations.

We will use several "well-known" lemmas about the distortion of angles under conformal maps and, in particular, the distortion of triangles pushed forward by a

conformal map. Since these facts were recorded and explained in [8], in the context of constructing triangulations, we give specific citations to that paper, although the relevant facts about conformal maps could be found elsewhere.

3 Conformal Maps

We start with the following simple lemma.

Lemma 3.1 *Suppose P is a polygon and $\Omega = \mathrm{Int}(P)$. Then there is a model domain Ω' with boundary P', and a conformal map $f\colon \Omega \to \Omega'$ which gives a bijection between the vertices of P and the infinite ends of Ω'.*

Proof This is a fairly standard fact and it follows from the Riemann mapping theorem and the Schwarz–Christoffel formula. Suppose $\phi\colon \mathbb{D} \to \Omega$ is conformal (such a map exists by the Riemann mapping theorem) and $\mathbf{z} = \{z_1, \ldots, z_n\} \subset \mathbb{T}$ are the pre-images of the vertices of P. Suppose the interior angles of P are $\boldsymbol{\alpha}\pi = \{\alpha_1\pi, \ldots, \alpha_n\pi\}$. Then the Schwarz–Christoffel formula says that ϕ is given by

$$\phi(z) = A + C\int^{z} \prod_{k=1}^{n}\left(1 - \frac{w}{z_k}\right)^{\alpha_k - 1} dw, \tag{3.1}$$

for some choice of constants A, C. See e.g. [15, 33, 36].

Let $\mathcal{I} = \{I_k\}$ be the connected components of $\mathbb{T} \setminus \mathbf{z}$. Choose two non-adjacent I_k's, and then choose three points near the center of each of the other $n-2$ elements of $\mathcal{I}$. Set $\alpha = 4/3$ at these points. For each z_k choose two points $z_k^{\pm}$ on either side z_k and set $\alpha = 1/2$ at these points. Then apply the Schwarz–Christoffel formula to get a polygon, as shown on the top of in Fig. 3. Take the limit as $z_k^{\pm} \to z_k$; the finite polygonal domains converge to the unbounded domain described in the lemma and illustrated in Fig. 3. The desired map $\Omega \to \Omega'$ is just the composition of ϕ^{-1} with this limit of Schwarz–Christoffel maps. □

Given a triangulation in Ω' we transfer it to a triangulation in P by mapping the vertices of each triangle and then connecting the images by line segments. The following shows that angles are not distorted very much (this is [8, Lem. 3.2]).

Lemma 3.2 *If $0 < \delta < 1/2$, f is a conformal map on a disk $D(z, r)$ and $T = \Delta ABC$ is a triangle inside $D(z, \delta r)$, then the triangle $f^*T = \Delta f(A) f(B) f(C)$ has angles that are within $O(\delta)$ of the corresponding angles of T.*

Corollary 3.3 *Suppose $f\colon \Omega \to \Omega'$ is a conformal map between the interiors of two domains. Suppose that $T \subset \Omega$ is a triangle of diameter $\epsilon > 0$, and that for some $z \in T$, $D(z, d) \cap \partial\Omega$ is empty or consists of a single line segment S such that $f(S)$ is a line segment in $\partial\Omega'$. Then f maps the vertices of T to the vertices of a triangle $T' \subset \Omega'$ whose angles are within $1 + O(\epsilon/d)$ of the corresponding angles of T.*

Proof If the intersection is empty, then Lemma 3.2 applies directly to $D(z, d)$. If the intersection is a line segment S as described, then f can be extended from $D(z, d) \cap \Omega$ to all of $D(z, d)$ by Schwarz reflection, and then Lemma 3.2 is applied. □

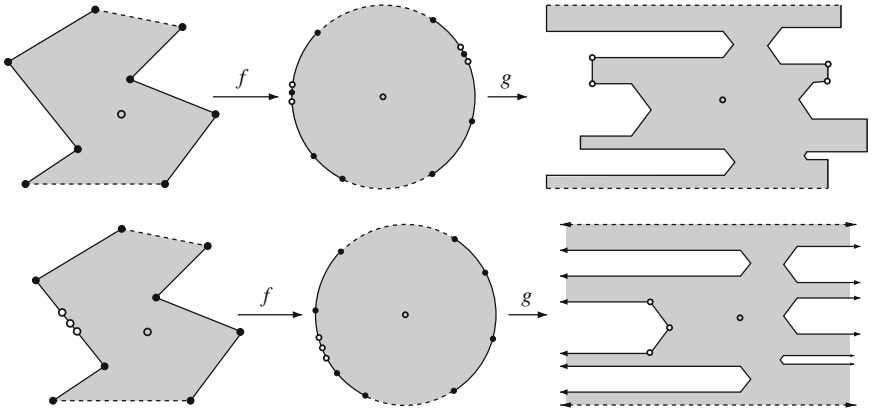

Fig. 3 Using the Schwarz–Christoffel formula, one can map the interior of any simple polygon to a subset of a strip as shown on top. By taking the preimages $z_k^{\pm}$ of the 90° corners to converge to z_k, we get a conformal map onto an unbounded model domain, as shown on the bottom

In particular, this corollary applies to the conformal map between a polygon and its model domain. Fix a large $M < \infty$. Suppose the nearly equilateral triangles in Ω' have diameter $\epsilon > 0$, and that ϵ is so small that each infinite end of P' has thickness $\geq M$. Applying Corollary 3.3 with $d = M\epsilon$ shows that for any triangle T' in Ω' that is distance $\geq M\epsilon$ from every vertex of P', the corresponding triangle in T has angles within a factor of $1 + O(1/M)$ of those of T, and hence it will also be nearly equilateral, if M is large enough. Therefore, we can transfer a nearly equilateral triangulation of the model domain to Ω. The image triangles are all close to equilateral by Lemma 3.2, except those near the 240°-vertices, but by choosing the triangulation fine enough we may assume the angles of these triangles are bounded by $67.5° + \epsilon$ for any $\epsilon > 0$. The 67.5° arises because near a 240° vertex $v \in P'$ in the boundary, the conformal map acts like $z^{3/4}$, sending the 240° angle on P' to 180° on P. The 60° angles that touch v are mapped to $(3/4) \cdot 60° = 45°$; the image triangle under the power map is isosceles, so each of the other two angles is $(180°–45°)/2 = 67.5°$. See Fig. 4. The conformal map $\Omega' \to \Omega$ is not equal to the power map, so the 67.5° may be slightly exceeded. However, taking a fine enough triangulation ensures all the image angles are less than 75°.

As noted above, the model domain can be written as a compact polygon plus a finite number of infinite ends that are each half-strips. Inside these half-strips the triangulation is equilateral but infinite. Also, in the half-strips the conformal map to Ω approximates an exponential map. In particular, a vertical segment connecting the horizontal sides of an end maps to a close approximation of a circular arc connecting, and orthogonal to, the two sides of P adjacent to the corresponding vertex of P. See Fig. 2. The infinite half-strip beyond the vertical segment maps to an approximate truncated sector in the region Ω. We inscribe a polygonal arc γ with M evenly spaced points on γ. This defines a polygonal sector. We will triangulate this sector with the desired angle bound, without adding any vertices to γ. This is described in Sects. 6 and 7.

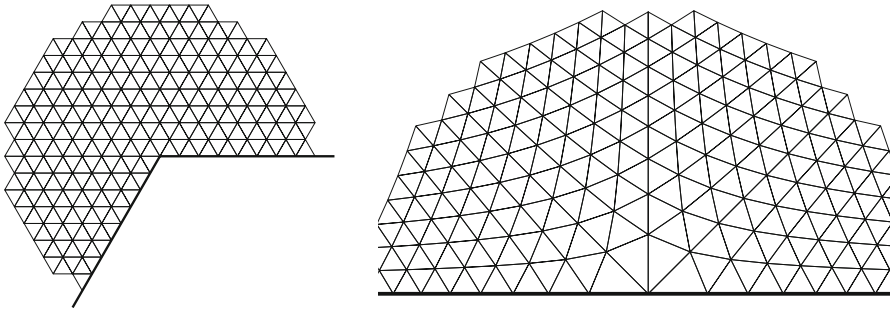

Fig. 4 Mapping an equilateral triangulation of a 240°. sector by $z \mapsto z^{3/4}$ gives a 67.5°-triangulation. The maximum occurs in the four triangles touching the origin

Remark 4 The methods of [8] can be used attain the 67.5° angle bound near the image of the 240° degree corner, not just approximate it. See [8, Lem. 6.3] for a precise statement describing of how this works. With more work, using the "420°-trick" from [8], the 67.5° bound can be further lowered to $(5/7) \cdot 90° \approx 64.2857°$, but we do not need the better estimate here. However, we will need to use the related "120°-trick" in the next section.

4 Interpolation Between Triangulations in a Strip

An infinite strip has several natural equilateral triangulations $\mathcal{T}_n$ determined by the number n of horizontal rows of triangles. See Fig. 5 where parts of $\mathcal{T}_6$ and $\mathcal{T}_{12}$ are illustrated. This figure also illustrates the two interpolation problems described in the paragraphs following Lemma 2.1.

First, the triangulations $\mathcal{T}_n$ do not contain vertical segments, and we will have to construct an explicit triangulation that "fills the gap" between part of $\mathcal{T}_n$ and the vertical end of a half-strip, i.e., fill in the left blank region in Fig. 5. This is easy to do, as shown in Fig. 6 (in our construction, we are free to choose the "width" of this region). Thus when we truncate the infinite ends of P' by vertical segments, the region between the equilateral triangulation and the segment can be triangulated with angles $\leq 72°$ as promised in Sect. 2. Corollary 3.3 applies, so the triangulation can be transferred from P' to P with all angles remaining below 75°.

The second problem illustrated in Fig. 5 is to interpolate between $\mathcal{T}_n$ and $\mathcal{T}_m$ for $n \neq m$. This is more difficult to deal with, and the problem will arise in our construction because each infinite end of the model domain has an equilateral triangulation that is determined by its "thickness", i.e., the number of horizontal rows triangles. When choosing the nearly equilateral triangulation of the model domain, the thickness of each end can be made as large as we wish by subdividing the triangulation, but we can't choose the thickness of each end independently. By interpolating between two different equilateral triangulations of a strip, we will be able to change the thickness of each end, independently of what happens in the other ends.

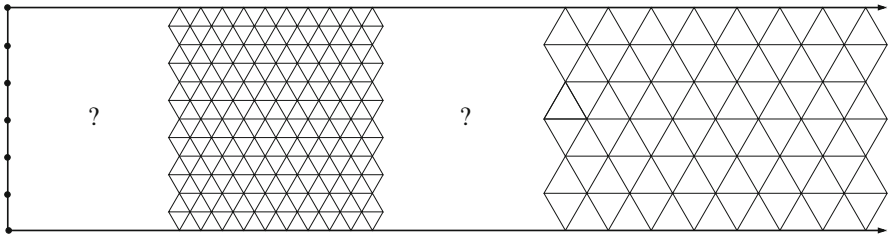

Fig. 5 Two problems involved with merging the triangulations. On the left we have to complete the triangulation between an equilateral triangulation and the end of a half-strip. On right we have to interpolate between two equilateral triangulations of different sizes. In our applications, we are free to choose the widths of the intermediate regions to be meshed

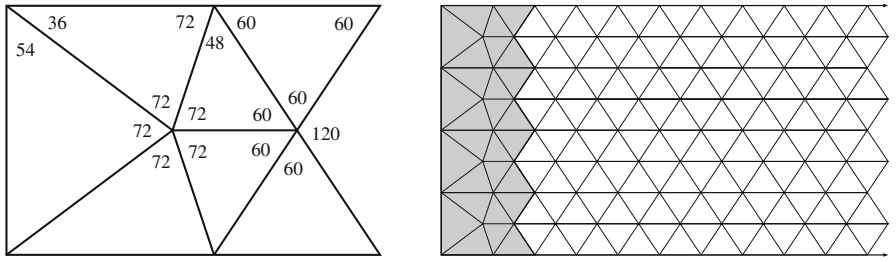

Fig. 6 On the left is a triangulation of an indented rectangle. Note that every angle is $\leq 72°$. On the right we show how it "fills in" between a partial equilateral triangulation of strip and the end of a half-strip

Lemma 4.1 *Given $N < \infty$ there is an $A < \infty$ such that if $n, m \geq N$ then there is a $72°$-triangulation $\mathcal{T}_{n,m}$ of $S = \mathbb{R} \times [0, 1]$ that equals $\mathcal{T}_n$ on $S \cap \{x < -A\}$ and that equals $\mathcal{T}_m$ on $S \cap \{x > A\}$.*

Proof Construct a "funnel strip", as illustrated on the top of Fig. 7, that has a equilateral triangulation that is n triangles thick in one direction and m triangles thick in the other direction. Map this to a strip as shown on the bottom of Fig. 7. If n, m are large enough, then the triangles in the image are all close to equilateral, except near the images of the corners. Near the image of the 240° interior corner, the image triangulation has angles bounded by 67.5°; the argument is the same as described in Sect. 3 for the behavior near the 240° angles in P' (recall Fig. 4). Near the 120° corner, a more complicated construction is needed.

Near the 120° corner, the conformal map acts like a power map $z \mapsto z^{3/2}$. This is made precise by [8, Lem. 6.2 and 6.3]. The image of the equilateral triangulation under this power map is shown in Fig. 8. Because only two triangles touch the corner in the funnel, the images of these triangles have 90° angles at the image of the corner. This is too large for our purposes. Near the image of the 120° angle in the funnel, the image triangulation must be replaced by another triangulation using only angles $\leq 72°$. This is accomplished by the "120°-trick" from [8]. See Fig. 9. The trick is made precise using the following result [8, Lem. 7.1].

Lemma 4.2 *Suppose $f : P' \to P$ is a conformal map between polygons that maps vertices to vertices. Suppose $f(v') = v$ where v' is a vertex of P' and v is a vertex*

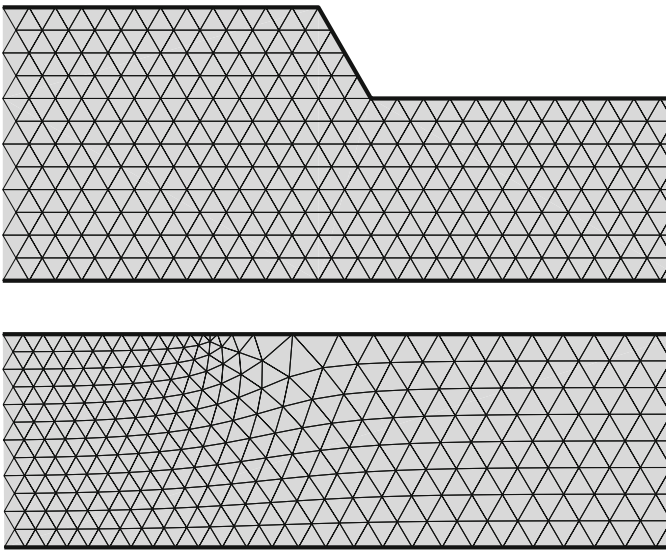

Fig. 7 We use a conformal map to transfer equilateral triangulation from a "funnel strip" to a true strip. Enlargements of the behavior near the 120° and 240° corners are illustrated on Figs. 4 and 8. These figures were produced with Driscoll's SC-Toolbox [14]

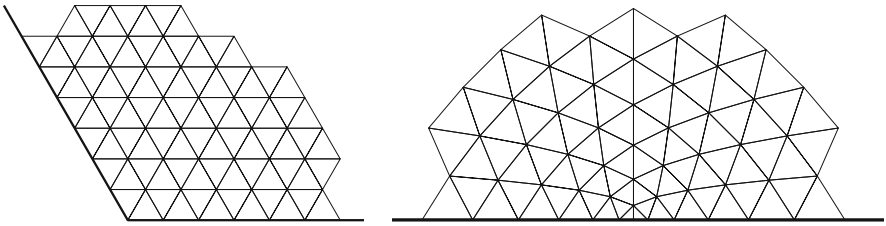

Fig. 8 Near the 120° corner, the conformal map acts like a power map $z \mapsto z^{3/2}$. The image triangulation contains two 90° angles

of P, with angles 120° *and* 180° *respectively. Suppose $\mathcal{T}$ is a nearly equilateral triangulation of P' and $f^*\mathcal{T}$ the image triangulation. If $\mathcal{T}$ is fine enough, then there is a neighborhood U of v and a triangulation $\mathcal{S}$ of P that equals $f^*\mathcal{T}$ outside U and every triangle of $\mathcal{S}$ touching U has all angles $\leq 72°$.*

Moreover, we can choose A so that the pushed forward triangulation in the strip is as close as we wish to $\mathcal{T}_n$ and $\mathcal{T}_m$ in the two components of $S \setminus [-A, A] \times [0, 1]$. Thus the pushed forward triangulation can be replaced with these in the components while keeping all angles, except those near the corners, close to 60°. This completes the proof of Lemma 4.1. □

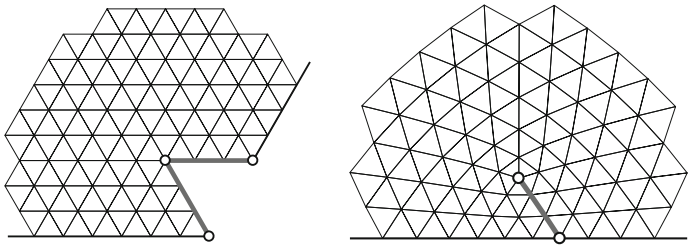

Fig. 9 The "120°-trick" from [8] creates a triangulation of a half-plane with maximum angle 72° (right side) by taking the conformal image of an equilateral triangulation of a 120°-sector with some triangles removed (left side). Two boundary arcs on the modified sector are identified as one internal arc γ in the new triangulation, and an interior vertex of degree 5 is created. The arc γ appears straight, but is actually slightly curved to ensure the image vertices on either side of γ match up (that this is possible is proved in [8]). The conformal map approximates $z^{3/2}$ near infinity, hence the new triangulation approximates the $z^{3/2}$-triangulation from Fig. 8 near infinity

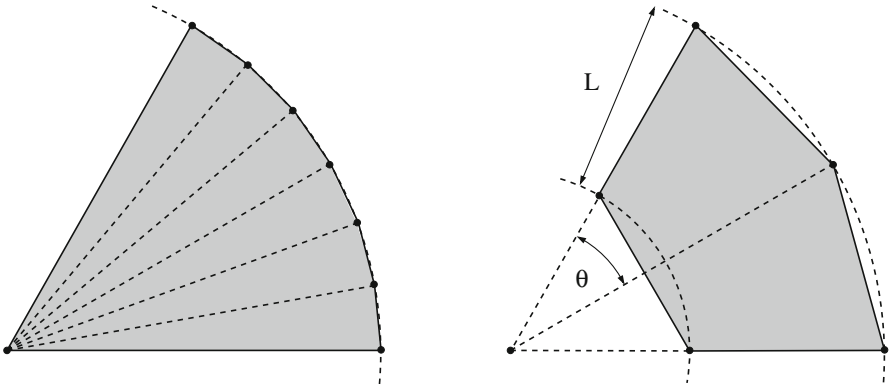

Fig. 10 On the left is a general polygonal sector. On the right is a truncated polygonal sector; in this case a pentagon, the case of greatest interest to us. We want to triangulate such pentagons with good angle bounds without adding any vertices to the "inner" and "outer" sides

5 Polygonal Sectors

A polygonal sector is a polygon with one vertex at the origin and the others inscribed on, and evenly spaced along, a circular arc centered at the origin. A truncated polygonal sector is the difference of two such regions corresponding to the same angular arc on two different radius circles. See Fig. 10.

We are most interested in sectors that are pentagons with one segment inscribed on the smaller circle and two on the larger circle. These pentagons are symmetric with respect to the angle bisector of the corresponding sector; we shall call these shapes "sector pentagons". See the right-hand side of Fig. 10. The side of the pentagon closest to the origin is the "inner" edge, the two farthest edges are the "outer" edges. The two other sides are the "radial" edges (they lie on rays through the origin). The "length" L of such a pentagon is the length of the radial edges. Note that in Fig. 10 we have defined θ to be half the angle of the sector; this is convenient for some formulas in

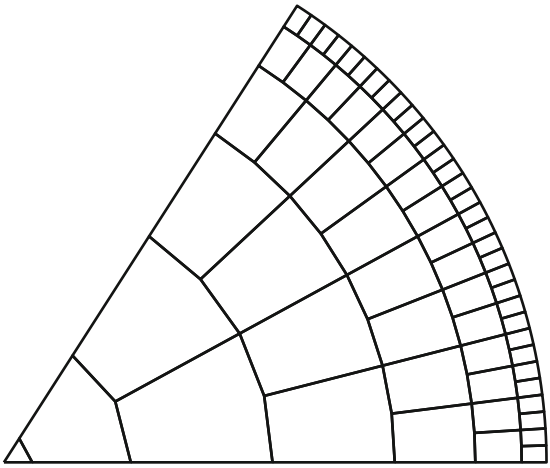

Fig. 11 A mesh of a polygonal sector into one triangle and several pentagons

later sections, and we will call θ the "sector angle". The rest of the paper is devoted to finding upper angle bounds for acute triangulations of symmetric pentagons that only place boundary vertices on the radial edges.

The importance of these pentagons is illustrated in Fig. 11, which shows how to mesh a polygonal sector with 2^n outer edges by a single isosceles triangle and $2^{n+1}-2$ pentagons. If each pentagon has a 75°-triangulation, and the vertices match up along common boundaries, then we obtain a triangulation of the whole polygonal sector. This will happen if the pentagon triangulations have no extra vertices on the inner or outer edges of the pentagon; if the triangulation is symmetric, then vertices on the radial edges match up automatically, and otherwise we can use reflected versions in alternate pentagons (note that pentagons in the same layer have the same shape).

Suppose v is a vertex of P where P has interior angle $\theta_v > 60°$. We divide the angle into equal sub-angles that are each in $(30°, 60°]$ and use the mesh in Fig. 11 to each of the corresponding sub-sectors. There are at most six triangles touching v, and each is isosceles with maximum angle $\leq 75°$. If $\theta_v \leq 60°$, then we do not subdivide the angle and we use a single copy of the mesh in Fig. 11. The isosceles triangle touching v will have two angles equal to $90° - \theta_v/2$, which will be $> 75°$ if $\theta_v < 30°$. For example, if P has angle 40° at v, the corresponding value of θ is 20°; if P has angle 100°, we will subdivide it into two sectors of angle 50° and apply the lemma twice with $\theta = 25°$.

There are at most six triangles touching any vertex v, and each is isosceles with maximum angle $\leq 75°$. Thus the sector mesh at a vertex v of P will be bounded by $k \cdot 2^j$ segments along its outermost edge, where $k \in \{1, \ldots, 6\}$ and j is as large as we wish. By Lemma 4.1 we can arrange for the triangulation in the corresponding end of P' to have exactly this thickness, so the conformal image of the triangulation in the end can be joined to the triangulation of the sector. Thus to prove Theorem 1.1, is only remains to verify the following result.

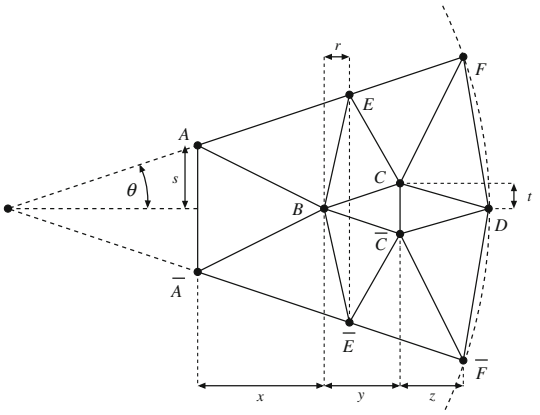

Fig. 12 The triangulation $\mathcal{T}(\theta)$ of a polygonal sector. The precise definition is given in the text. We assume $0 \le \theta \le 30°$

Lemma 5.1 *For each* $0 < \theta \le 30°$ *there is a choice of length* L *such that the corresponding symmetric sector pentagon has a* $75°$*-triangulation, with no vertices on the inner or outer edges. The triangulation is symmetric with respect to the pentagon's axis of symmetry.*

The proof is given in the next two sections. Both sections make use of a particular triangulation of a sector pentagon. See Fig. 12 for the abstract graph. The points labeled A, B, C, D, E, F are defined in terms of positive parameters r, s, t, x, y, z as follows (using complex notation):

$$\begin{aligned} A = is, \quad B = x, \quad C = x + y + it, \\ E = x + r + i[s + (x + r)\tan\theta], \\ F = x + y + z + i[s + (x + y + z)\tan\theta], \end{aligned}$$

and D on the real line is defined by the condition that $\angle EFD = 90° - \theta/2$; this makes ΔAFD isosceles. If the figure were translated so that the line containing AF hit the real axis at the origin O, then this angle condition would be equivalent to $|DO| = |FO|$; we don't state it this way to include the case $\theta = 0$ where AF is parallel to the real axis. Here XY denotes the segment with endpoints X and Y, and $|XY|$ is its length. The triangulation is symmetric with respect to the real line, and for X in the plane, $\overline{X}$ denotes its complex conjugate (its reflection over the x-axis).

As motivation for what follows, we fix a value of θ, set $s = 1$ and then use a computer to search for values of r, t, x, y, z that are close to minimizing the maximum angle. A graph of the maximum angle found for each value of θ is shown in Fig. 13. The graph appears to have a piecewise linear structure, but we do not investigate this here. More importantly, the plot indicates that the maximum angle is bounded above by $75°$, attained at the right-hand endpoint $30°$.

To actually prove the $75°$ upper bound, it is convenient to break the proof into two ranges: $\theta \in [0, 18°]$ and $\theta \in [18°, 30°]$. For the latter range, we will define the

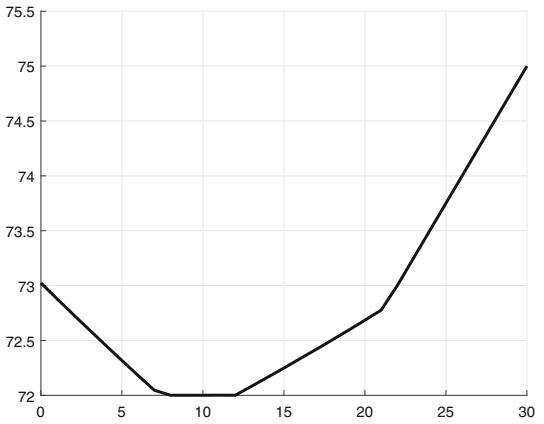

Fig. 13 The maximum angle used in the triangulation $\mathcal{T}(\theta)$ for $0 \le \theta \le 30°$ based on a computerized search for parameters. This indicates the estimate $\le 75°$ is true with the maximum attained at $30°$

triangulation by specifying certain angles in terms of θ. From these, the values of several other angles can be deduced by elementary geometry. All these angles are easily verified to be $\le 75°$ for all θ in the given range. However, there are four angles with values that do not have simple formulas in terms of θ. These angles we can compute numerically for a finite set of θs between $18°$ and $30°$, and to estimate their values between these points we have to bound the derivative of these angles with respect to θ. We then choose the gaps between the evaluations to be so small that the maximum over the discrete evaluations is within $.1°$ of the maximum over the whole interval (and the discrete maximum will be ≤ 74.5).

A similar numerical strategy will be used in Sect. 7 to deal with the interval $[0, 18°]$, but there monotonicity will be used instead of a derivative bound.

6 Lemma 5.1: $18° \le \theta \le 30°$

We start by specifying the triangulation in terms of the sector angle θ. For $18° \le \theta \le 30°$, set $\delta = 30° - \theta$. Note that $0 \le \delta \le 12°$. Recall $\angle EFD = 90° - \theta/2$. We set:

$$67.5° \le \angle DC\overline{C} = \angle DCF = \angle FCE = 75° - \frac{\delta}{4} = 67.5° + \frac{\theta}{4} \le 75°,$$
$$72° \le \angle BCE = 72° + \frac{\delta}{4} \le 75°, \qquad \angle AB\overline{A} = 72°.$$

These values, and the symmetric ones in the lower half-plane, determine the triangulation completely. Several other angles can be computed easily from these using the fact that the angles of triangle sum to $180°$. For example,

$$\angle CD\overline{C} = 180° - 2\angle DC\overline{C} = 180° - 2\left(67.5° + \frac{\theta}{4}\right) = 45° - \frac{\theta}{2},$$

so

$$30^\circ \le \angle CD\overline{C} = 30^\circ + \frac{\delta}{2} = 45^\circ - \frac{\theta}{2} \le 45^\circ.$$

The following estimates are proven by similar arguments and left to the reader:

$$\begin{aligned}
60^\circ \le \angle CDF = 60^\circ + \frac{\delta}{4} &= 67.5^\circ - \frac{\theta}{4} \le 63^\circ,\\
63^\circ \le \angle BC\overline{C} = 63^\circ + \frac{\delta}{2} &= 78^\circ - \frac{\theta}{2} \le 69^\circ,\\
\angle CFD &= 45^\circ,\\
30^\circ \le \angle EFC = 30^\circ + \frac{\delta}{2} &= 45^\circ - \frac{\theta}{2} \le 46^\circ,\\
67.5^\circ \le \angle CEF = 75^\circ - \frac{\delta}{4} &= 67.5^\circ + \frac{\theta}{4} \le 75^\circ,\\
42^\circ \le \angle CB\overline{C} = 54^\circ - \delta &= 24^\circ + \theta \le 54^\circ,\\
54^\circ \le \angle BAE &= 36^\circ + \theta \le 66^\circ.
\end{aligned}$$

Of the angles given above, the maximum is $75^\circ - \delta/4$ for $24^\circ \le \theta \le 30^\circ$, and $72^\circ + \delta/4$ for $18^\circ \le \theta \le 24^\circ$. In either case, the maximum angle is less than 75° for $\theta \in [18^\circ, 30^\circ]$. Note that since $\angle CEF = 75^\circ - \delta/4 = \angle FCE$, the triangle ΔFEC is isosceles and hence $|EF| = |CF|$. Also note that all the angles listed above depend linearly on θ, and the derivative of the angle with respect to θ is always has value in $\{0, \pm 1/4, \pm 1/2, \pm 1\}$. In particular, the absolute value of the derivative is always ≤ 1.

There are only four other angles to consider: $\angle ABE$, $\angle AEB$, $\angle EBC$, and $\angle BEC$. These are not easily solvable in terms of θ, but they do satisfy the equations

$$\begin{aligned}
\angle ABE + \angle EBC &= 180^\circ - 36^\circ - \frac{\angle CB\overline{C}}{2} = 120^\circ - \frac{\theta}{2},\\
\angle AEB + \angle BEC &= 180^\circ - \angle CEF = 112.5^\circ - \frac{\theta}{4},\\
\angle AEB + \angle ABE &= 180^\circ - \angle BAE = 150^\circ - \theta,
\end{aligned}$$

so that knowing any one of these four angles tells us the other three. We can compute these numerically for a finite number of θs, but in order to control the values between the evaluated points we have estimate the derivative of these angles in terms of θ. The sum formulas above easily imply the absolute values of the derivatives (with respect to θ) of any two of these angles differ by at most 2, e.g. $\frac{d}{d\theta}\angle AEB = -\frac{d}{d\theta}\angle ABE = 1$. Hence it is enough to bound one of these derivatives; we will focus on $\angle BEC$.

Since angles are preserved by similarities, we can normalize the triangulation as θ varies so that the vertex F if fixed, and the segment FC has length 1. Then C remains on the unit circle around F and the angle between CF and the horizontal direction is $\theta + \angle EFC = 45^\circ + \theta/2$. Thus C moves at most at rate $1/2$ in θ. (All derivatives of trig functions are computed in radians, despite our using degrees to specify angles.)

The segment EF makes an angle θ with the horizontal and the length of this segment can be computed using the Law of Sines:

$$|EF| = |EC| \cdot \frac{\sin \angle ECF}{\sin \angle EFC} = \frac{\sin(82.5^\circ - \theta/4)}{\sin(45^\circ - \theta/2)}.$$

If we compute the derivative using the quotient rule, the denominator will be larger than $\sin(30^\circ)^2 = 1/4$ and the denominator is a sum of two terms, each of which is a product of three terms that are less than 1 in absolute value (two trigonometric functions and the derivative of the angle with respect to θ). Thus the derivative of $|EF|$ is bounded by $2/(1/4) = 8$ in absolute value. Hence E can move with rate at most $\sqrt{1+8^2} < 9$.

The segment BC makes angle $12^\circ + \theta/2$ with the horizontal, and since $|EC| = 1$, $|BC|$ can be computed by applying the Law of Sines three times as

$$|BC| = \frac{\sin \angle B\overline{C}C}{\sin \angle CB\overline{C}} \cdot \frac{\sin \angle CD\overline{C}}{\sin \angle C\overline{C}D} \cdot \frac{\sin \angle CDF}{\sin \angle CFD}.$$

Differentiating using the product rule and quotient rules, gives us a sum of three terms. Each term has two of the factors left alone and the third differentiated. As above, the numerator of the differentiated term has absolute value at most 2. Thus the derivative of $|BC|$ is bounded by

$$\frac{2 \cdot \sin \angle CD\overline{C} \cdot \sin \angle CDF}{(\sin \angle CB\overline{C})^2 \cdot \sin \angle C\overline{C}D \cdot \sin \angle CFD} + \frac{2 \cdot \sin \angle BC\overline{C} \cdot \sin \angle CDF}{\sin \angle CB\overline{C} \cdot (\sin \angle C\overline{C}D)^2 \cdot \sin \angle CFD}$$
$$+ \frac{2 \cdot \sin \angle BC\overline{C} \cdot \sin \angle CD\overline{C}}{\sin \angle CB\overline{C} \cdot \sin \angle C\overline{C}D \cdot (\sin \angle CFD)^2} \leq 3.7474 + 3.6786 + 3.9265 < 12,$$

where we have used the lower bounds

$$\angle C\overline{C}D \geq 72^\circ, \qquad \angle CB\overline{C} \geq 45^\circ, \qquad \angle CFD \geq 45^\circ,$$

and the upper bounds

$$\angle BC\overline{C} \leq 69^\circ, \qquad \angle CD\overline{C} \leq 45^\circ, \qquad \angle CDF \leq 63^\circ,$$

that we computed earlier from our assumption that $18^\circ \leq \theta \leq 30^\circ$. Thus the vector $C - B$ changes at a rate of bounded by $\sqrt{1+12^2} \leq 13$. Since C changes at most at rate $1/2$, this implies B changes at rate at most 14. Finally, note that

$$|EC| = |EF| \cdot \frac{\sin \angle EFC}{\sin \angle CEF} \geq \sin \angle EFC \geq \sin 30^\circ \geq \frac{1}{2}$$

and

$$|EB| \geq \mathrm{Im}(E) \geq |EC| \cdot \sin(\angle BCE + \angle BC\overline{C} - 90^\circ)$$

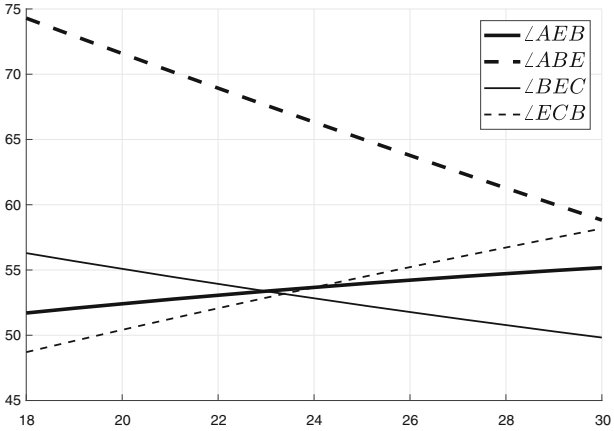

Fig. 14 Plots of the four angles $\angle ABE$, $\angle AEB$, $\angle EBC$, and $\angle BED$ evaluated at intervals of .001°. The maximum is 74.2977°. The variation of these angles within the gaps is $\leq .1°$

$$\geq |EC| \cdot \sin\left(45° + \frac{3}{4}\delta\right) \geq |EC| \cdot \frac{1}{\sqrt{2}} > \frac{1}{3}.$$

Thus the $C - E$ and $B - E$ each move at rate at most 20 and the lengths of these vectors are both at least $1/3$. Therefore the size of $\angle BEC$ changes at a rate $\leq 3(20 + 20) = 120$, and so the other three angles each change at rate ≤ 122.

Note that $1/100$ degrees is $\pi/180000 < 1/5000$ radians. Thus each of our angles changes by less than .1 radians over such an interval, and hence by less than .1 degrees. Figure 14 plots the four angles in question for θ between 18° and 30° with gaps of $(1/1000)°$. The maximum is $\approx$ 74.2977 attained by $\angle ABE$ at $\theta = 18°$, so the four special angles being considered are all $\leq 74.4°$. Thus all the angles are $\leq 75°$, completing the proof of Lemma 5.1 for $\theta \in [18°, 30°]$.

7 Lemma 5.1: $0° \leq \theta \leq 18°$

We now turn to triangulating polygonal sectors with angles smaller than 18°. We will use a monotonicity argument to show that the maximum angle needed for all $0 \leq \theta \leq 18°$ can be bounded by the maximum angles needed for a certain finite set of triangulations corresponding to a finite set of values $\theta \in [0, 18°]$. Thus the argument reduces to another "brute force" computation.

We use the same combinatorial triangulation as in the last section; see Fig. 12 and the definitions of $A, B, \ldots, F$ at the end of Sect. 5. For each fixed angle θ, each choice of x, y, z, r, t determines a triangulation. By plugging in and evaluating the angles, we get an upper angle bound for triangulating the corresponding truncated θ-sector. We do not claim the bounds we obtain are optimal, although they are probably close to optimal for the given combinatorics (although other combinatorial triangulations may give better bounds).

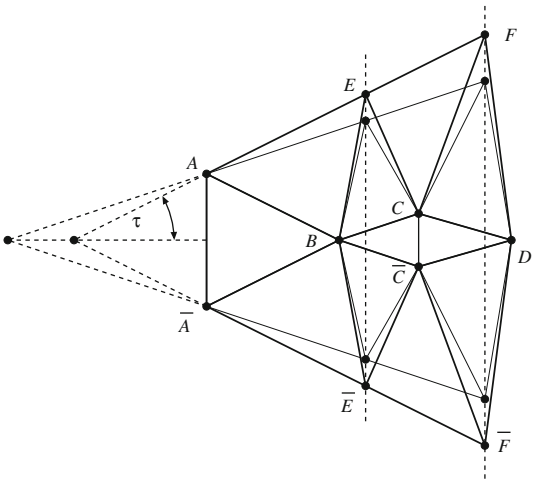

Fig. 15 The first variation. We move the vertices $E, \overline{E}, F, \overline{F}$ in Fig. 12 vertically so that they lie on a new line making a larger angle with the horizontal. The other points are not moved. Every angle changes monotonely. Since D is not moved, the new figure is not quite a polygonal sector. This is fixed in Fig. 16

We will do this explicit calculation for a finite number of angles $0 = \theta_0 < \ldots < \theta_n = 18°$. To obtain bounds that are valid for all angles, we will give a 1-parameter family of triangulations of polygonal sectors between angles θ_k and θ_{k+1}. For each such interval we use a computer search to find a good set of parameters x, y, z, r, t to define the starting triangulation $\mathcal{T}_k$ with sector angle θ_k. For each sector angle $\theta_k \leq \tau \leq \theta_{k+1}$ we describe how to move $\mathcal{T}_k$ in two steps (the first moves vertices E and F, and the second moves vertex D). We obtain a triangulation of a truncated sector with angle τ, and then use similar moves to change this to a triangulation of a sector with angle θ_{k+1}. We will show with a monotonicity argument that every angle for the triangulation at τ can be bounded above by some angle in one of four associated triangulations. Thus the angle bound for any $\tau \in [0, 18°]$ is bounded by the maximum angle from a finite set of triangulations, all of which we compute.

The first family of perturbed triangulations is shown in Fig. 15. We draw the lines through A and $\overline{A}$ that makes an angle $\tau > \theta$ with the horizontal. The points $E, F, \overline{E}, \overline{F}$ are moved vertically to lie on this line. The new positions are denoted $E', F', \overline{E}', \overline{F}'$. All other points are left fixed. Triangles involving only the vertices $A, \overline{A}, B, C, \overline{C}, D$ are not changed. The angles $\angle BAE, \angle CBE, \angle BCE, \angle DCE$, and $\angle DCF$ increase with τ. By symmetry, so do the corresponding angles in the lower half-plane. The remaining angles decrease with τ. However, this is not a triangulation of a polygonal sector of angle τ, since D is in the wrong place.

In Fig. 16, we show how to move D to D', in a way that makes the region a polygonal sector. This motion affects three triangles, hence nine angles. For an angle that is not effected, the final value is the same as the value after the first step. Since angles change monotonely in the first step, the final values for any $\tau \in [\theta_k, \theta_{k+1}]$ is bounded by the angle values at one of the endpoints after the first step.

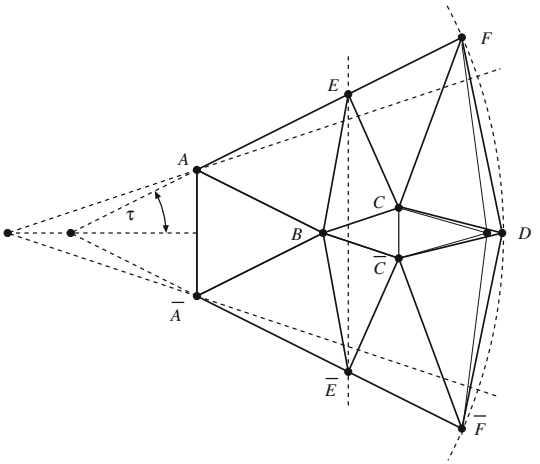

Fig. 16 This is the same as Fig. 15, except that D has been moved to the right, so the region becomes a polygonal sector. Only the angles of triangles containing D are changed, and all change monotonely

Similarly, no angle in the triangle $CD\overline{D}$ changes in the first step, and they all change monotonely in the second step, so their final values for any τ are bounded between their values when $\tau \in \{\theta_k, \theta_{k+1}\}$.

The only angles that require some thought are those that change in opposite directions in the first and second steps. For example, consider angle $\angle CDF$. This increases in the first step and decreases in the second. Thus its final value is less than its value between the two steps, and since the first step is increasing in τ, this intermediate value is less than the value we would get by setting $\tau = \theta_{k+1}$. In symbols,

$$\angle CD'F'(\tau) \leq \angle CDF'(\tau) \leq \angle CDF'(\theta_{k+1}).$$

Similarly,

$$\angle D'CF'(\tau) \leq \angle DCF'(\tau) \leq \angle DCF'(\theta_{k+1}).$$

The angle $\angle CFD$ is slightly different: since the second step increases this angle, we can't bound it above by its intermediate value. Instead, we observe that we can get to the final configuration by a different path: move D first, then move $E, F, \overline{E}, \overline{F}$. The intermediate triangulation is shown in Fig. 17. The first step of this alternate motion increases $\angle CFD$, and the second step decreases it. Thus

$$\angle CF'D'(\tau) \leq \angle CFD'(\tau) \leq \angle CFD'(\theta_{k+1}).$$

We have only dealt with angles in the upper half-plane, but by symmetry the same bounds hold in the lower half-plane.

We have now shown that every polygonal sector of angle $\tau \in [\theta_k, \theta_{k+1}]$ can be triangulated with an upper angle bound that is bounded by the maximum angle of one of four triangulations:

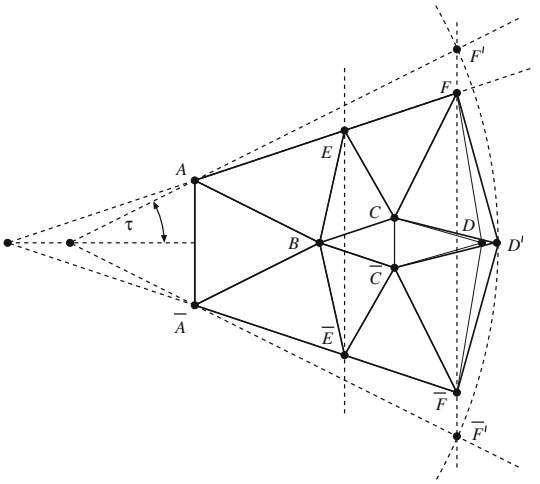

Fig. 17 This is the second variation: we move D but not E or F. As we move D, all the angles of triangles containing D change monotonely. To make this a polygonal sector, we then have to move E, F and their conjugates vertically

Table 1 This gives the maximum angle used on the four different meshes corresponding to the intervals $[\theta, \theta + 1]$ for $\theta = 0, 1, \ldots, 17$)

θ	max angle	x	y	z	t	r
0	74.774	1.376	0.812	0.611	0.248	0.306
1	74.572	1.411	0.826	0.636	0.254	0.298
2	74.358	1.409	0.839	0.662	0.261	0.289
3	74.185	1.488	0.854	0.691	0.268	0.281
4	74.007	1.541	0.870	0.721	0.275	0.271
5	73.791	1.500	0.880	0.747	0.281	0.260
6	73.595	1.498	0.891	0.775	0.286	0.248
7	73.400	1.472	0.899	0.802	0.291	0.234
8	73.305	1.405	0.931	0.830	0.303	0.255
9	73.315	1.478	0.997	0.877	0.324	0.301
10	73.314	1.518	1.066	0.924	0.346	0.352
11	73.290	1.465	1.123	0.962	0.365	0.399
12	73.255	1.376	1.181	0.996	0.384	0.451
13	73.317	1.378	1.215	1.036	0.403	0.464
14	73.373	1.372	1.251	1.077	0.422	0.482
15	73.437	1.370	1.288	1.119	0.443	0.498
16	73.502	1.368	1.325	1.163	0.465	0.515
17	73.573	1.366	1.364	1.209	0.488	0.533

All these numbers are less than 75° and therefore Lemma 5.1 holds in this interval range. We have used intervals of length 1 to save space; using shorter intervals would give smaller angle bounds, closer to the graph in Fig. 13. The other columns give the parameter values that define $A, B, \ldots, F$, so that the calculations can be recreated (the values have been normalized so $s = 1$)

- $\mathcal{T}_k$,
- $\mathcal{T}_k$ with only E, F, $\overline{E}$, $\overline{F}$ moved,
- $\mathcal{T}_k$ with only D moved,
- $\mathcal{T}_k$ with all five points moved.

Moving the points in this particular way is not optimal, but does give an easy-to-analyze family of triangulations whose maximum angles can be bounded by a finite, computable list of numbers. We can get better bounds by making the gaps between the θ_k smaller; this means we only make small perturbations from configurations we think are close to optimal. For this paper, I took the gap to be $1°$. Table 1 shows the maximal angles used in each of the four triangulations, giving an upper bound that is valid for all sector angles $\theta \in [k°, (k+1)°]$, $k = 0, \ldots, 17$. The maximum angle is $\approx 74.4774° < 75°$, so the lemma is proven, and hence so is Theorem 1.1.

References

1. Baker, B.S., Grosse, E., Rafferty, C.S.: Nonobtuse triangulation of polygons. Discrete Comput. Geom. **3**(2), 147–168 (1988)
2. Bern, M., Eppstein, D.: Mesh generation and optimal triangulation. In: Computing in Euclidean Geometry. Lecture Notes Ser. Comput., vol. 1, pp. 23–90. World Sci. Publ., River Edge (1992)
3. Bern, M., Eppstein, D., Gilbert, J.: Provably good mesh generation. J. Comput. Syst. Sci. **48**(3), 384–409 (1994)
4. Bern, M., Mitchell, S., Ruppert, J.: Linear-size nonobtuse triangulation of polygons. Discrete Comput. Geom. **14**(4), 411–428 (1995)
5. Bern, M., Plassmann, P.: Mesh generation. In: Handbook of Computational Geometry, pp. 291–332. North-Holland, Amsterdam (2000)
6. Bishop, C.J.: Optimal angle bounds for quadrilateral meshes. Discrete Comput. Geom. **44**(2), 308–329 (2010)
7. Bishop, C.J.: Nonobtuse triangulations of PSLGs. Discrete Comput. Geom. **56**(1), 43–92 (2016)
8. Bishop, C.J.: Optimal triangulation of polygons (2021). https://www.math.stonybrook.edu/~bishop/papers/opttri.pdf
9. Bishop, C.J.: Uniformly acute triangulations for PSLGs. Discrete Comput. Geom. (2023). https://doi.org/10.1007/s00454-023-00524-x
10. Brandts, J., Korotov, S., Křížek, M., Šolc, J.: On nonobtuse simplicial partitions. SIAM Rev. **51**(2), 317–335 (2009)
11. Burago, Yu.D., Zalgaller, V.A.: Polyhedral embedding of a net. Vestnik Leningrad. Univ. **15**(7), 66–80 (1960). (in Russian)
12. Burago, Yu.D., Zalgaller, V.A.: Isometric piecewise-linear embeddings of two-dimensional manifolds with a polyhedral metric into $\mathbb{R}^3$. Algebra i Analiz **7**(3), 76–95 (1995). (in Russian)
13. Cassidy, Ch., Lord, G.: A square acutely triangulated. J. Recreational Math. **13**(4), 263–268 (1980/1981)
14. Driscoll, T.A.: Algorithm 843: improvements to the Schwarz–Christoffel toolbox for MATLAB. ACM Trans. Math. Softw. **31**(2), 239–251 (2005)
15. Driscoll, T.A., Trefethen, L.N.: Schwarz–Christoffel Mapping. Cambridge Monographs on Applied and Computational Mathematics, vol. 8. Cambridge University Press, Cambridge (2002)
16. Edelsbrunner, H.: Triangulations and meshes in computational geometry. Acta Numer. **9**, 133–213 (2000)
17. Eppstein, D.: Acute square triangulation (2021). https://www.ics.uci.edu/~eppstein/junkyard/acute-square/
18. Erten, H., Üngör, A.: Computing acute and non-obtuse triangulations. In: 19th Canadian Conference on Computational Geometry (Ottawa 2007), pp. 205–208. http://cccg.ca/proceedings/2007/09a2.pdf
19. Gerver, J.L.: The dissection of a polygon into nearly equilateral triangles. Geom. Dedicata **16**(1), 93–106 (1984)

20. Hangan, Th., Itoh, J., Zamfirescu, T.: Acute triangulations. Bull. Math. Soc. Sci. Math. Roumanie (N.S.) **43**(**91**)(3–4), 279–285 (2000)
21. Itoh, J.: Acute triangulations of sphere and icosahedron. In: 1st International Symposium on Differential Geometry (Sakado 2001). Josai Math. Monogr., vol. 3, pp. 53–62. Josai University, Sakado (2001)
22. Itoh, J., Yuan, L.: Acute triangulations of flat tori. Eur. J. Comb. **30**(1), 1–4 (2009)
23. Itoh, J., Zamfirescu, T.: Acute triangulations of the regular icosahedral surface. Discrete Comput. Geom. **31**(2), 197–206 (2004)
24. Itoh, J., Zamfirescu, T.: Acute triangulations of the regular dodecahedral surface. Eur. J. Comb. **28**(4), 1072–1086 (2007)
25. Kopczyński, E., Pak, I., Przytycki, P.: Acute triangulations of polyhedra and $\mathbb{R}^N$. Combinatorica **32**(1), 85–110 (2012)
26. Křížek, M.: There is no face-to-face partition of $\mathbb{R}^5$ into acute simplices. Discrete Comput. Geom. **36**(2), 381–390 (2006)
27. Li, J.Y.S., Zhang, H.: Nonobtuse remeshing and mesh decimation. In: 4th Eurographics Symposium on Geometry Processing (Cagliari 2006), pp. 235–238. Eurographics Association, Goslar (2006)
28. Lindgren, H.: Dividing a square into acute-angled triangles. Aust. Math. Teach. **18**, 14–15 (1962)
29. Maehara, H.: On acute triangulations of quadrilaterals. In: Japanese Conference on Discrete and Computational Geometry (Tokyo 2000). Lecture Notes in Comput. Sci., vol. 2098, pp. 237–243. Springer, Berlin (2001)
30. Maehara, H.: Acute triangulations of polygons. Eur. J. Comb. **23**(1), 45–55 (2002)
31. Manheimer, W.: Dissecting an obtuse triangle into acute triangles (solution to problem E1406). Am. Math. Mon. **67**(9), 923 (1960)
32. Melissaratos, E.A., Souvaine, D.L.: Coping with inconsistencies: a new approach to produce quality triangulations of polygonal domains with holes. In: 8th Annual Symposium on Computational Geometry (Berlin 1992), pp. 202–211. ACM, New York (1992)
33. Nehari, Z.: Conformal Mapping. Dover, New York (1975)
34. Ruppert, J.: A new and simple algorithm for quality 2-dimensional mesh generation. In: 4th Annual ACM-SIAM Symposium on Discrete Algorithms (Austin 1993), pp. 83–92. ACM, New York (1993)
35. Saraf, S.: Acute and nonobtuse triangulations of polyhedral surfaces. Eur. J. Comb. **30**(4), 833–840 (2009)
36. Trefethen, L.N., Driscoll, T.A.: Schwarz–Christoffel mapping in the computer era. In: International Congress of Mathematicians (Berlin 1998), vol. 3. Doc. Math., pp. 533–542. Deutsche Mathematiker-Vereinigung, Berlin (1998)
37. Yuan, L.: Acute triangulations of polygons. Discrete Comput. Geom. **34**(4), 697–706 (2005)
38. Yuan, L., Zamfirescu, C.T.: Acute triangulations of doubly covered convex quadrilaterals. Boll. Unione Mat. Ital. **10-B**(3), 933–938 (2007)
39. Yuan, L., Zamfirescu, T.: Acute triangulations of flat Möbius strips. Discrete Comput. Geom. **37**(4), 671–676 (2007)
40. Zamfirescu, C.: Acute triangulations of the double triangle. Bull. Math. Soc. Sci. Math. Roumanie (N.S.) **47**(**95**)(3-4), 189–193 (2004)
41. Zamfirescu, C.T.: Survey of two-dimensional acute triangulations. Discrete Math. **313**(1), 35–49 (2013)